Desalination and Water Treatment
www.deswater.com

doi: 10.5004/dwt.2023.29200

282 (2023) 246–257
January

Activation of *Luffa cylindrica* with particulate matter for the removal of fluoride ions from aqueous solutions in a fixed-bed adsorption column

J.J. García-Sánchez[a,*], M. Solache-Ríos[b], M.C. Maldonado-Orozco[c], R. Sánchez-Orozco[a], O. Soriano-Vargas[a], J.J. García-García[d]

[a]*Tecnológico Nacional de México, Tecnológico de Estudios Superiores de Jocotitlán, Carretera Toluca-Atlacomulco Km 44.8, Ejido de San Juan y San Agustín Jocotitlán, 50700 Jocotitlán, México, Phone: 712 1231313; emails: jjuangs1@gmail.com (J.J. García-Sánchez), r.sanchez@tesjo.edu.mx (R. Sánchez-Orozco), sorianovo78@gmail.com (O. Soriano-Vargas)*
[b]*Instituto Nacional de Investigaciones Nucleares, Depto. de Química. Carretera México-Toluca S/N, La Marquesa, C.P. 52750 Ocoyoacac, Estado de México, México, Phone: 55 53297200; email: marcos.solache@inin.gob.mx*
[c]*Universidad Autónoma de Chihuahua, Circuito Universitario 1, Campus Uach II, 31125 Chihuahua, Chih., México, Phone: 614 442 9500; email: cmaldona@uach.mx*
[d]*Instituto Potosino de Investigación Científica y Tecnológica, A.C. Camino a la Presa San José 2055. Col. Lomas 4 sección CP 78216 San Luis, S.L.P., Phone: 444 8342000; email: jose.garcia@ipicyt.edu.mx*

Received 22 May 2022; Accepted 6 December 2022

ABSTRACT

Luffa sponge (fibrous network obtained from mature dried *Luffa cylindrica*) was activated using particulate materials to increase its adsorption capacity for fluoride ions from aqueous solution. The activation of the *Luffa cylindrica* with hydroxyapatite (HA) on the surface presented the best efficiency in the removal of fluoride ions. The presence of hydroxides (OH^-) as active groups in the *Luffa cylindrica* structure are responsible for adsorption. In this work, the results of bioadsorption tests of fluoride ions with *Luffa cylindrica*-HA in fixed-bed columns are presented. The depth of mass transfer zone increased from 5.5 to 11.0 cm, with bed volumes of 4.32 and 8.64 cm^3, respectively. The results were treated with various fixed-bed models (Thomas, Yoon–Nelson, Dose–Response and Weibull distribution). The results obtained showed that breakthrough time increases as the bed height increases. The bed capacity was 2.4 mg/g, with the bed depth, influent flow rate and influent concentration of 5.5–11.0 cm, 1 mL/min, and 5 mg/L, respectively. The breakthrough curve matched the Thomas, Yoon–Nelson, Dose–Response, and Weibull, models. The Weibull distribution model was used to predict the breakthrough curve from the experimental results. The results were well fitted to this model and the adsorption capacity was calculated. The study of the operating parameters of the column on a laboratory scale can be used to simulate the potential performance of the adsorbent and extrapolate the results to a pilot scale or larger.

Keywords: Luffa cylindrica; Hydroxyapatite; Fluoride ions

1. Introduction

The living organisms depends upon the purity of water; therefore, water pollution is a major problem; especially in the regions where people depend on groundwater. The quality of water has been deteriorated, due to pollution by dissolved metallic and non-metallic chemical species. Among these pollutants, anionic species like fluoride in groundwater has been recognized as one of the serious problems worldwide. The World Health Organization

* Corresponding author.

(WHO) has recommended 1.5 mg/L as the maximum limit level in drinking water. Consumption of water with fluoride ions above this limit could induce several health problems like dental fluorosis and a long-term exposure causes another type of fluorosis called skeletal fluorosis [1]. Besides, fluoride is also known to have an adverse effect on the cardiovascular, central nervous, digestive, immune, renal and respiratory systems [2]. Hence, it is important to supply water with safe fluoride ions levels. Various methods like chemical precipitation, adsorption, electrocoagulation, reverse osmosis and electrodialysis have been reported to remove fluoride from drinking water [3–7].

Adsorption is the most efficient and cost-effective method to remove fluoride ions in comparison with other methods. Various types of biosorbents, polymer resins/fibers/membranes, organics, different metal oxides, composites, and more recently a variety of nanomaterials have been studied for the removal of fluoride ions from aqueous solutions [8–14].

The application of nanoparticles on the removal of contaminants from water has allowed the synthesis of new materials that are more selective, efficient, and therefore better adsorbents. Nanomaterials have been used to remove fluoride from water, excellent results with high efficiencies have been reported [15].

Sairam Sundaram et al. [16] used nanometric compounds: hydroxyapatite ($Ca_{10}(PO_4)_6(OH)_2$) and chitin (polysaccharide) to remove fluoride ions. Nano-hydroxyapatite/chitin composite possesses higher defluoridation capacity (2,840 mg F^-/kg) than nano-hydroxyapatite (1,296 mg F^-/kg).

Patel et al. [17] prepared colloidal CaO particles by the sol–gel method to remove fluoride ions from aqueous solutions in a batch system, and they obtained almost a complete elimination of fluoride (98%).

Kang et al. [18] investigated the efficiency of a new adsorbent for fluoride removal from water. The adsorbent was synthesized by calcining magnesia (MgO) with pullulan, an extracellular water-soluble microbial polysaccharide. The adsorption capacity was 4,537 mg/kg at 30°C and pH 7.0, using the initial concentration of 10 mmol/L fluoride solution.

Zhao et al. [19] prepared nanoparticles consisting of hydrated aluminum oxide embedded in Fe_2O_3 nanoparticles (Fe_3O_4@$Al(OH)_3$), they reported that the adsorption capacity calculated by the Langmuir equation was 88.48 mg/g at pH 6.5.

Liu et al. [20] investigated the feasibility of using synthetic siderite for F^- removal from aqueous solution. The synthetic siderite showed a high adsorption capacity for F^- removal, which was up to 1.775 mg/g in batch with an adsorbent dosage of 5 g/L and an initial F^- concentration of 20 mg/L at 25°C.

Zhang et al. [21] used waste phosphogypsum to prepare and apply hydroxyapatite nanoparticles to remove fluoride ions from aqueous solutions, particles from 20 to 60 nm were obtained with high purity. The maximum adsorption capacity found by means of the Langmuir–Freundlich model were 19.742, 26.108, 36.914, and 40.818 mg/g at temperatures of 298, 308, 318, and 328 K, respectively.

Tariq et al. [22] reported the use of biomass *Ficus religiosa* in untreated and xanthate treated forms for the Cd(II) ions removal in a fixed-bed column. Breakthrough time and exhaust times increased (67.5–390 min and 292.5–1,852.5 min) (97.5–442.5 min and 345–1,920 min) for unmodified and modified materials, respectively. The modified material exhibited a capacity of 55.20 mg/g and the unmodified material of 13.33 mg/g.

The composition of fibrous net obtained from the dry *Luffa cylindrica* is mainly cellulose and in contact with water is negatively charged, a quality that allows positive particles to be attracted to their structure. The activation of *Luffa cylindrica* with particulate material could be an effective alternative adsorbent for the removal of fluoride ions from water.

Due to the small size of the particles (micro or nano), it is difficult to separate by conventional processes. Therefore, this research was focused on synthesizing particulate mineral materials such as elemental iron, calcite, alumina, or hydroxyapatite supported on an organic material (*Luffa cylindrica*).

In this work, the removal of fluoride ions in a bed column system was analyzed, and the data obtained from the tests were evaluated by using empirical kinetic models. One model used was the Weibull distribution. This model is flexible due to the inclusion of a shape parameter (β) in addition to the scale parameter (α), which allows its application in various systems. The Weibull distribution can be used as a model to correlate asymmetric adsorption curves and the Weibull function generates *S*-shaped curves for $\beta > 1$. The parameters, α and β, can be easily determined using a spreadsheet program [23].

In order to adequately describe the fluoride removal kinetics in an adsorption column, the values of the parameters α and β of the Weibull model were determined. This model presents a logistic function similar to the Thomas equation in relation to the mass transfer [24], the following two relationships were proposed: β = kinetic constant (min^{-1}) and $\alpha = q_W m/C_o Q$.

2. Materials and methods

2.1. Materials

Luffa sponge was used as a support for metallic particles, this material consists of a fibrous network obtained from the mature dried *Luffa cylindrica* fruit. The sponge was purchased from the local market. The fruit of this *Cucurbitaceae* is a fibrous endocarp, which is composed of cellulose (60%), hemicellulose (30%) and lignin (10%) [25]. Sodium carbonate, sodium nitrate, sodium hydroxide, calcium nitrate, aluminum sulfate, sodium carbonate, calcium hydroxide, iron(III) chloride hexahydrate, sodium borohydride and ammonium hydroxide were provided by Sigma-Aldrich (MO, USA). Ethanol and phosphoric acid were purchased from Fisher Scientific Chemicals (MA, USA).

2.2. Preparation of activated Luffa cylindrica with particulate matter

The method for the preparation of the particulate matter and their deposition onto *Luffa cylindrica* is schematically depicted in Fig. 1.

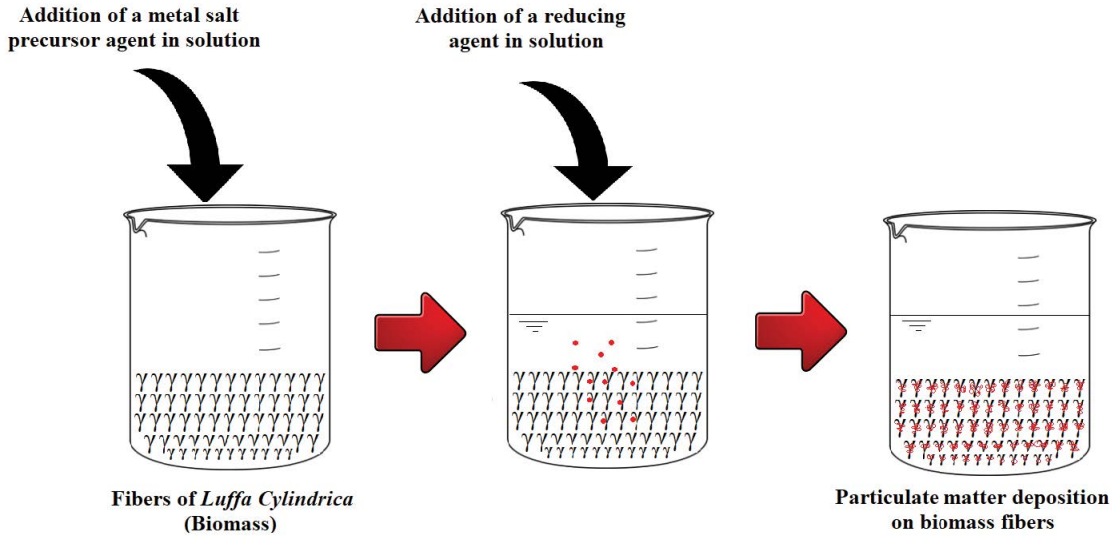

Fig. 1. Schematic representation of the conventional deposition/reduction method for the preparation of supported particles on *Luffa cylindrica*.

Activated bioadsorbents were prepared by the addition of a metal salt to the *Luffa cylindrica*, followed by the addition of a reducing agent, to obtain particulate matter by the deposition/reduction technique on *Luffa cylindrica*. The particulate material obtained is nano-sized, due to the reduction process.

2.2.1. Preparation of Luffa cylindrica

The *Luffa cylindrica* was washed with abundant distilled water and dried in an oven at 60°C for 24 h. Subsequently, it was ground and sieved to a particle size between 0.3 and 0.2 mm.

2.2.2. Synthesis and deposition of particulate material on Luffa cylindrica

2.2.2.1. Calcite ($CaCO_3$) biomaterial

Separately, 0.1 M Na_2CO_3, 0.2 M $NaNO_3$, and 0.2 M NaOH solutions were prepared as precursor agents, these solutions were mixed and added to a mass of 10 g of *Luffa cylindrica*. The reducing agent was added dropwise, which was a 0.1 M solution of $Ca(NO_3)_2$, under continuous stirring and constant temperature of 30°C. The phases were separated by filtration and the solid was washed three times with distilled water. The activated biomaterial was dried at 60°C and labeled as *Luffa cylindrica*-Ca [26].

2.2.2.2. Alumina (Al_2O_3) biomaterial

10 g of *Luffa cylindrica* was mixed with 100 mL of a 0.03 M $Al_2(SO_4)_3$ solution, then 100 mL of the reducing agent (1.0 M Na_2CO_3) was added dropwise. The resulting solution was kept at room temperature for 12 h under constant stirring. Then it was filtered and the solid was washed three times with distilled water. The activated biomaterial was dried at 60°C and labeled as *Luffa cylindrica*-Al [27].

2.2.2.3. Elemental iron (Fe) biomaterial

1.35 g of $FeCl_3{\cdot}6H_2O$ were dissolved in a solution containing 60 mL of ethanol and 20 mL of distilled water and mixed with 10 g of *Luffa cylindrica*. 0.3783 g of sodium borohydride were dissolved in 100 mL of distilled water. This reducing agent solution was added dropwise to the precursor, which was constantly stirred, then the mixture was stirred for another 20 min, then the mixture was filtered and the solid was washed three times with ethanol. The activated biomaterial was dried at 60°C and labeled as *Luffa cylindrica*-Fe [28].

2.2.2.4. Hydroxyapatite biomaterial

100 mL of a 0.3 M H_3PO_4 solution was dropwise added to an equal volume of a 0.5 M $Ca(OH)_2$ solution containing 10 g of *Luffa cylindrica*. The pH was kept above 10 by adding NH_4OH at constant temperature of 25°C, the mixture obtained was kept under stirring for 24 h, then the mixture was filtered and the solid was washed several times with distilled water, finally the activated biomaterial was dried at 60°C and labeled as *Luffa cylindrica*-HA [29].

2.3. Characterization

The microstructures, composition, morphology, and functional groups present in the natural and activated *Luffa cylindrica* were analyzed by means of scanning electron microscopy (SEM) and infrared spectroscopy, respectively. For SEM observations, the materials were mounted directly on the holders and then observed at 10 and 20 kV in a JEOL JSM 5900LD electron microscope (ININ, México). Before the analysis, the samples were coated with a thin layer of gold by using the sputtering technique, to increase conductivity, avoiding charge accumulation and possible sample degradation. The microanalysis was done with an EDS (energy-dispersive X-ray spectroscopy) system.

The Fourier-transform infrared spectroscopy (FTIR) study was performed by using a Fourier Varian transform infrared absorption spectrometer (FTIR Varian 640-IR) with diamond base and RTA (reflectance total attenuated) accessory to identify functional groups present in the samples before and after activation of the biomaterial. The spectra were recorded in the range of 4,000 to 500 cm^{-1}.

2.4. Determination of the fixed-bed porosity

The study of the transfer of fluid through porous beds, which relates the residence time of the fluid as a consequence of passing through the bed of particles, considers porosity as a measurable characteristic in an adsorption column. Moret-Fernández and López [30] proposed a simple method to estimate the porosity of a biomaterial.

Porosity is defined as the ratio between the volume of the porous fixed-bed space and the total volume of the bed. The porosity of the fixed-bed was determined as follows: the fixed-bed was dried at 60°C for 2 h, a weighed quantity of the material was placed in a column and the volume was measured, then the column was filled with distilled water and it was left until the liquid fills the internal pores of the fixed-bed. Once saturated, the unfilled volume of the column was measured and this volume is the volume of the pore space.

The fixed-bed porosity (ε) and density (ρ) were calculated from Eqs. (1) and (2), respectively.

$$\varepsilon = \frac{V_i}{V_T} \tag{1}$$

$$\rho_r = \frac{m}{V_r} \tag{2}$$

where V_i is the volume of the fixed-bed pore space in the column, V_T is the total volume of the bed (V_i + V_r), V_r is the volume of the solid particles in the fixed-bed, m is the mass of the dry fixed-bed and ρ_r the density of the material.

2.5. Fluoride measurements

The fluoride concentrations in the remaining solutions were measured with a selective ion electrode (ISE301F) by using a total ionic strength adjustment buffer solution (TISAB II with CDTA (trans-1,2-diaminocyclohexanetetraacetic acid, monohydrate)) to eliminate the interference of complexing ions.

2.6. Adsorption experiments

The experiments were carried out in batch mode to determine the adsorption capacities. 10 mL of fluoride solution (5 mg/L) and 0.1g of dried bioadsorbent were shaken for 24 h at 30°C. The samples were decanted, and the residual fluoride ions concentrations were measured with a selective ion electrode; each experiment was done in duplicate. The amount of the fluoride ions adsorbed (Adsorption capacity, AC) and removal percentage from solution were calculated by applying Eqs. (3) and (4), respectively:

$$q = \frac{\left(C_o - C_t\right)}{m} \times V \tag{3}$$

$$\text{Adsorption yield}(\%) = \frac{\left(C_o - C_e\right)}{C_o} \times 100 \tag{4}$$

where q refers to the amount of fluoride ions adsorbed by the bioadsorbent (mg/g); C_o is the initial fluoride ion concentration (mg/L), C_t is the final concentration (mg/L), V corresponds to the volume of aqueous solution (L), m is the mass (g) of bioadsorbent and C_e is the fluoride ion concentration in solution (mg/L) at equilibrium.

2.7. Column experiments

The fixed-bed column tests were only done with the biomaterial activated with hydroxyapatite, since it was the material that showed the highest efficiency on the adsorption of fluoride ions (Table 1).

Table 1
Elemental compositions and fluoride adsorption yield of the natural and activated *Luffa cylindrica*

Element (%)	*Luffa cylindrica*	*Luffa cylindrica*-Fe	*Luffa cylindrica*-Ca	*Luffa cylindrica*-Al	*Luffa cylindrica*-HA
C	51.5	43.8	45.0	30.3	29.2
O	45.9	34.8	46.9	45.1	35.5
Cl	1.4	1.8	0.9	0.5	0.5
Na	–	–	1.8	18.5	0.2
S	–	–	–	2.2	–
P	–	–	–	–	8.7
Fe	–	17.2	–	–	–
Al	0.8	2.3	0.3	2.9	1.0
Ca	0.4	–	5.1	0.6	24.8
Adsorption capacity (mg/g)	0.0	0.0	0.0	0.37	0.49
Adsorption (%)	0.0	0.0	0.0	73.4	98.7

The column studies were conducted to evaluate the effect of different bed weights on the breakthrough curves. Fixed-bed column experiments were performed by using a borosilicate glass column of 9 mm internal diameter and 20 cm high. The column was packed with activated *Luffa cylindrica* and the experiments were carried out using a solution of 5 mg/L of fluoride ions (pH = 6.4), a flow rate of 1 mL/min, 0.5, and 1.0 g of *Luffa cylindrica*-HA with bed depths of 5.5 and 11.0 cm, respectively. To keep the flow rate constant, a Masterflex model 77200-60 Peristaltic Pump was used.

The influent solutions were passed in down-flow mode through the bed; the flow rate was checked periodically during the experiments to assure uniformity on the hydraulic retention time during the experiment. Aliquots of effluent were collected at time intervals and the fluoride ions concentrations and pH were measured.

2.8. Desorption

50 mL of a 0.1 M NaOH solution were added to 0.5 g of fluoride-loaded *Luffa cylindrica*-HA (1.1 mg/g), material obtained after the adsorption process. The mixture was shaken at 150 rpm for 12 h, then the solution was centrifuged and the supernatant was collected to analyze the concentration of fluoride ions desorbed from *Luffa cylindrica*-HA. The desorption procedure was repeated three times.

3. Results and discussion

3.1. Capacities of the bioadsorbents for the removal of fluoride ions

The results show that the natural and activated *Luffa cylindrica* with calcite and elemental iron did not remove any fluoride ions from the solution. It was shown by elemental analysis and electron microscopy that the material (*Luffa cylindrica*) was modified with the chemical precursors, but they did not adsorb any fluoride ions, perhaps due to the little or no ionic affinity between the species. García-Sánchez et al. [31] reported similar behavior using iron oxides modified with calcium sulfate, where the removal of fluoride ions from aqueous solution was negligible.

The biomaterial activated with alumina and hydroxyapatite presented efficiency values for the removal of fluoride ions of 73.4% and 98.7%, respectively. In both cases, the ionic exchange between the OH^- species and the F^- could be responsible for the removal efficiencies.

Other works that have used hydroxyapatite reported high adsorption efficiencies. Zhang et al. [21] reported 99% efficiency for a fluoride solution with a concentration of 10 mg F^-/L and 0.3 g of adsorbent. He et al. [10] used hydroxyapatite nanowires as a membrane to the elimination of fluoride ions and reported efficiencies of 98%.

According to these results, only the material that presented the best adsorption capacity was used for the fixed-bed column system.

3.2. Characterization of the activated and natural Luffa cylindrica

3.2.1. Scanning electron microscopy

Fig. 2a shows the natural *Luffa cylindrica* with a macroscopic fibrous morphology, along the fibers presents certain interconnections. Fig. 2b shows parts of cellulosic fiber that form the *Luffa cylindrica* structure; cellulose fibers are seen, heterogeneously, cracked and fractured.

Elemental X-ray maps were generated, considering F and HA. The procedure was as follows: an area of interest was identified in the sample using the images provided by SEM. Subsequently, the qualitative analysis of the chemical elements of the selected area was performed, where the signals generated by backscattered electrons and characteristic X-rays were detected. The energies corresponding to the elements of interest (F and Ca) were selected. The composition of the element was transformed into maps where each color code represents the analyzed element (Fig. 3b and c).

SEM images of hydroxyapatite-activated *Luffa cylindrica* (HA) reveal the formation of a layer around the *Luffa cylindrica* and scattering between non-impregnated particles (Fig. 3). Fluoride ions were observed in the layer observed on the *Luffa cylindrica* (Fig. 3b), suggesting the presence of calcium oxide or calcium hydroxide and their possible electrostatic interaction with fluoride ions.

Fig. 3c and d revealed the presence of fluoride ions, dispersed on the *Luffa cylindrica* fiber (Fig. 3a). Possible electrostatic attraction or ionic substitution effects could play important roles on the adsorption process.

The physicochemical characteristics of hydroxyapatite, such as its composition, structure, texture, and surface

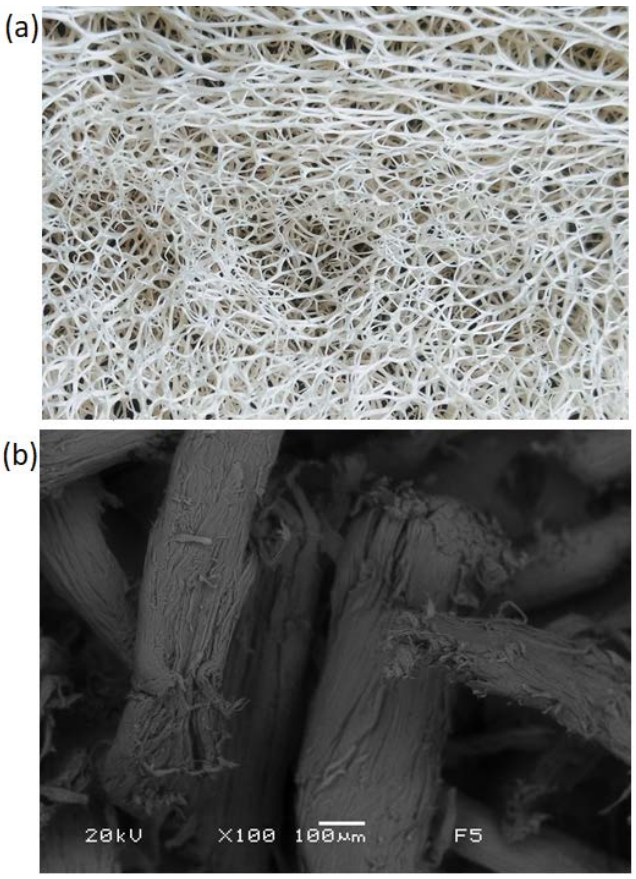

Fig. 2. (a, b) Macroscopic and microscopic morphologies of the natural *Luffa cylindrica*.

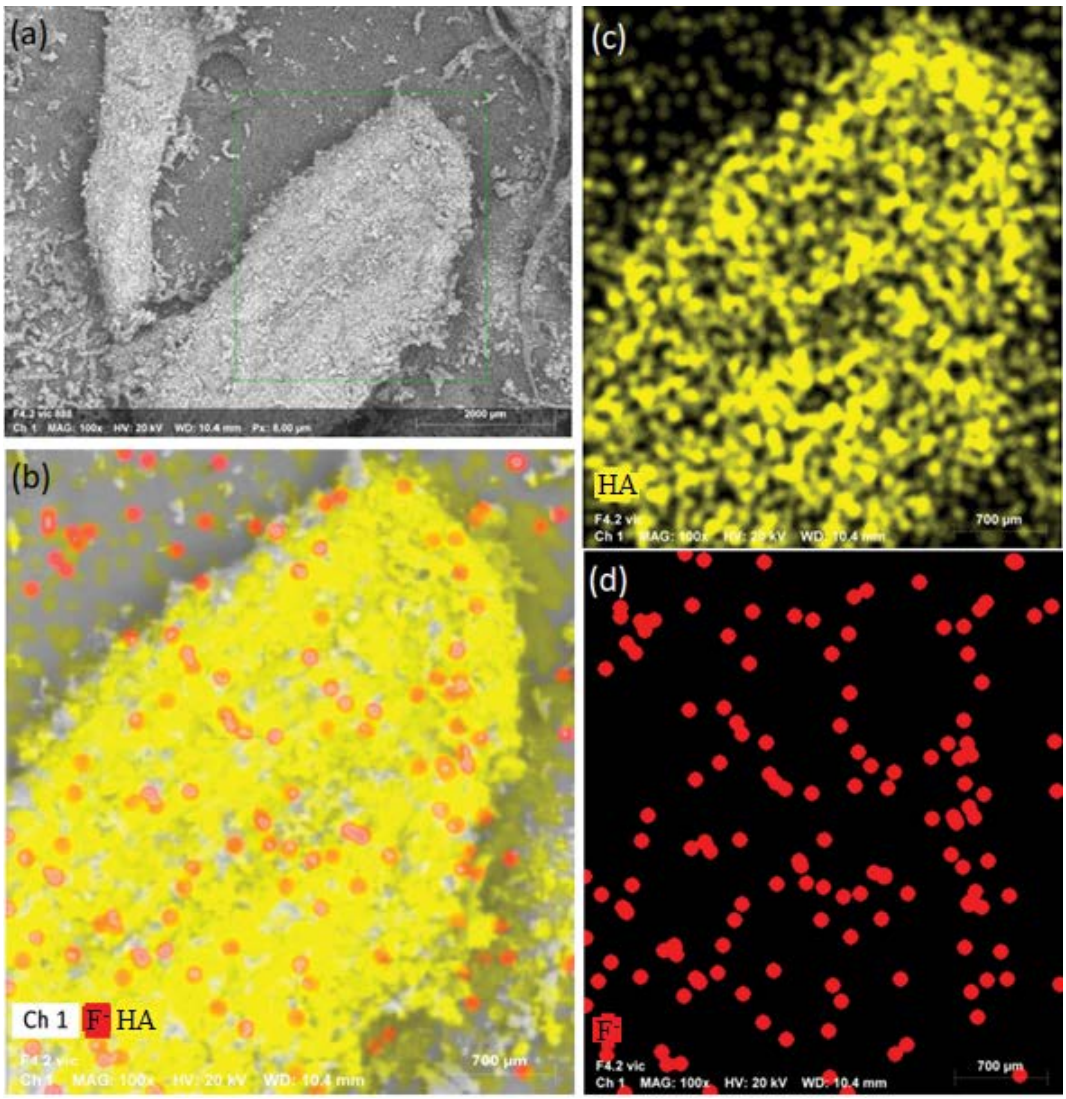

Fig. 3. Images of aggregate of hydroxyapatite: (a) SEM image, (b) compositional maps for F^- contained in the HA, (c) compositional maps for HA, and (d) compositional maps for F^-.

properties in the *Luffa cylindrica*, does the *Luffa cylindrica*-HA material the most suitable in the adsorption process. The elemental analysis of the activated bioadsorbents was determined by using the EDS, the results showed 17.2%, 5.1%, and 2.9% of Fe, Ca and Al for *Luffa cylindrica*-Fe, *Luffa cylindrica*-Ca and *Luffa cylindrica*-Al, respectively, the activated material with HA showed a greater amount of Ca (24.8%) and the presence of phosphorus (8.7%) characteristic of the HA (Table 1).

3.2.2. Fourier-transform infrared spectroscopy analysis

Fig. 4 shows the FTIR spectrum of activated and natural *Luffa cylindrica*. The FTIR spectrum of the activated *Luffa cylindrica* fiber (Fig. 4a) shows characteristic bands of hydroxyapatite. Intensive peaks at 563 and 1,026 cm^{-1} could indicate the presence PO_4^{3-} groups, and the peaks of 1,404 and 1,444 cm^{-1} correspond to CO_3^{2-}, representative of hydroxyapatite [32]. The peaks at 3,652 and 601 cm^{-1} are assigned to OH^- [33]. The peak at 874 cm^{-1} corresponds to out of plane bending mode of the CO_3^{2-} [33].

The FTIR spectrum of natural *Luffa cylindrica* fiber (Fig. 4b) shows a peak at 3,343 cm^{-1} assigned to the hydroxyl groups of cellulose, hemicellulose, involved in hydrogen bonds [34]. The 2,899 cm^{-1} band is due to the C–H stretching in methyl and methylene groups in cellulose and hemicellulose components [35]. The absorption peak at 1,720 cm^{-1} corresponds to C–O stretching of the carboxyl group of hemicellulose present in the fiber [36]. The band around 1,606 cm^{-1} was associated with C–C and C–O stretching in the aromatic ring, characteristic of lignin [37]. The band at 1,234 cm^{-1} is assigned to the C–O groups on the surface of the biomass, while that at 1,119 cm^{-1} corresponds to the stretching of the antisymmetric C–OR–C bridge (cellulose) [38,39]. The 1,086 cm^{-1} band is attributed to the anhydroglucose (cellulose) ring [39]. Peaks between 1,069 and 1,001 cm^{-1}

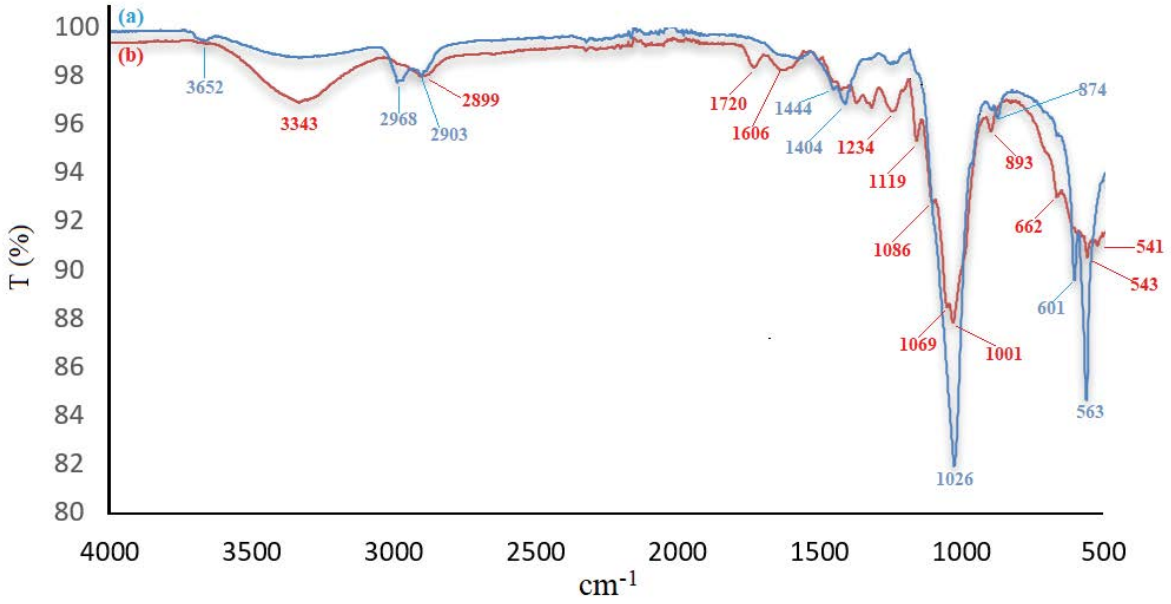

Fig. 4. Infrared spectrum: (a) activated *Luffa cylindrica* and (b) natural *Luffa cylindrica*.

are indicative of C–OR (cellulose) stretching, while the band at 893 cm^{-1} could be attributed to antisymmetric, out-of-phase stretching of the ring [38].

3.3. Column kinetic study

The physical characteristics of the fixed-bed were porosity 60%, density 0.3 g/L, depletion rate 2 g/L (90% saturation), the contact time increases as the weight of the fixed-bed increases, the values found were 4.31 and 8.64 min for 0.5 and 1.0 g, respectively.

3.3.1. Breakthrough curve

The breakthrough curve shows the behavior of fluoride ions adsorbed from solution by the fixed-bed column. It is expressed in terms of adsorbed fluoride concentration or normalized concentration defined as the ratio between the fluoride concentration in the effluent and the concentration of fluoride in the influent (C/C_o) as a function of the time or volume of the effluent for a given height of the bed.

Fig. 5a shows the breakthrough curves for the adsorption of fluoride ions with different bed depths. The permissible limit recommended by the WHO [40] is 1.5 mg/L and, this value was considered as the breakthrough point. It can be observed that breakthrough increases as the bed height increases, due to the accessibility of more adsorption sites. The breakthrough point corresponds to C/C_o = 0.3 (1.5 mg/L) and it was found at 92.0 and 202.7 mL of treated fluoride solution with bed weight of 0.5 and 1.0 g, respectively.

Fig. 5b shows that increasing the mass of the adsorbent, the service area of the bed increases, and by increasing the area, the interaction between the fluoride ions and the active sites of the *Luffa cylindrica*-HA also increases, and the treated volume of solution. When the fluoride solution passes through the adsorbent material, reaching its lower part, the F^- ions cannot longer be completely adsorbed due to the saturation of the material. After a while, the column is completely saturated or exhausted and the adsorption of F^- ions does no longer take place and the C/C_o ratio is close to one. In this area, the adsorption process is complete, the concentration of fluoride ions varies from the initial concentration to zero and the saturation of the adsorbent material is completed. As the volume of fluoride solution passes through the column, an adsorption zone beginning to be defined where mass transfer occurs. The mass transfer zone (MTZ) is the active surface of the *Luffa cylindrica*-HA biomaterial, where the F^- ions adsorption takes place.

3.3.2. Kinetic models of fixed-bed column adsorption

The values of the mass transfer coefficients in the solid phase were calculated from the experimental data and the models of Thomas, Yoon–Nelson, Dose–Response and Weibull distribution (Table 2).

The Thomas model assumes a Langmuir adsorption–desorption kinetic process, deriving from the fact that the speed driving force obeys second-order reversible reaction kinetics. This model also assumes a constant separation factor applicable to favorable or unfavorable isotherms [41,42]. From the results obtained (Table 3), the constant K_{Th} decreases as the deep of the column increases, due to the difference between the concentration of F^- adsorbed on the material and the F^- concentration in the solution. At the same time, it is observed that the determination coefficients R^2 and the adsorption capacities have about the same value.

Yoon–Nelson model does not require detailed data on the characteristics of the adsorbate, the type of adsorbent, or the physical properties of the adsorption bed [43]. This model assumes that the decrease rate of the adsorption

probability for each adsorbate molecule is proportional to the adsorption probability of the adsorbate and the penetration probability of the adsorbate into the adsorbent [44].

In Table 3, it is observed that increasing the mass of the adsorbent, the time required for rupture (τ) increases as well, but not directly proportional to the mass of the adsorbent. It could also be seen that the rate constant (K_{YN}) decreases with increasing the mass of the adsorbent, possibly due to the increase of the bed height.

The τ values of the model (119.56 and 294.37 min) were very close to the values obtained, reaching 50% adsorbate breakthrough (110 and 250 min), with 0.5 and 1.0 g of adsorbent material, respectively.

The Dose–Response model is used to describe column adsorption, and its importance lies in the fact that it describes the complete rupture curve with great accuracy, minimizing the resulting error in the adsorption kinetics of the column, especially that presented by the model of Thomas at the beginning and end of the breakdown curve [24,45,46].

Dose–Response constants increase with increasing bed height. On the other hand, the q_{d-r} values are very similar to those obtained by the other models, which confirms the validity of the experiment.

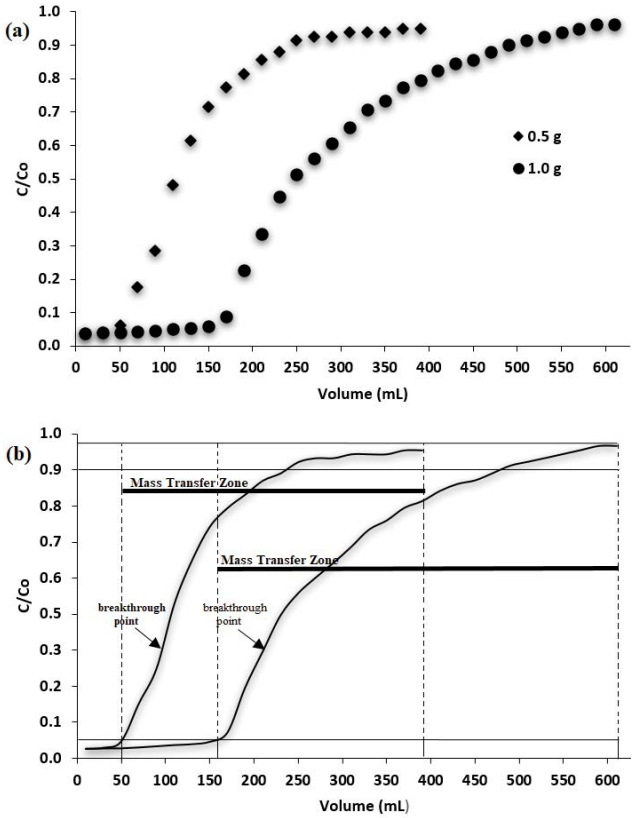

Fig. 5. Breakthrough curves using *Luffa cylindrica*-HA with two amounts of adsorbent material: (a) breakthrough curves on F^- removal in the fixed-bed column, and (b) representation of the breakthrough curves with mass transfer zone (MTZ).

Table 3
Parameters calculated form the experimental data and the kinetic models

Models	Parameters	Bed weight (m)	
		0.5 g	1.0 g
Thomas	K_{Th} (mL/mg·min)	0.004	0.002
	q_{Th} (mg/g)	1.4	1.5
	R^2	0.928	0.928
Yoon–Nelson	K_{YN} (1/min)	0.017	0.012
	τ (min)	120	294
	R^2	0.927	0.928
Dose–Response	a (1/mL)	3.0	3.9
	q_{d-r} (mg/g)	1.2	1.4
	R^2	0.992	0.984
Weibull distribution	b (1/min)	1.8	2.6
	α (min)	151	337
	q_W (mg/g)	1.5	1.7
	R^2	0.953	0.930

Table 2
Summary of the models used to evaluate the breakthrough curves

No.	Model	Linear equation	Parameters
(5)	Thomas	$\ln\left(\frac{C_o}{C_e}-e\right)=\frac{K_{Th}q_{Th}m}{Q}-K_{Th}C_o t$	Constants K_{Th} and q_{Th} were determined from a plot (plot omitted) of $\ln(C_o/C_e-1)$ vs. t at a given flow rate
(6)	Yoon–Nelson	$\ln\left(\frac{C_e}{C_o-C_e}\right)=K_{YN}t-K_{YN}\tau$	Values of K_{YN} and τ are obtained from the slope and intercept of the linear plots (plot omitted) of $\ln(C_e/C_o-C_e)$ vs. t
(7)	Dose–Response	$\ln\left(\frac{C_e}{C_o-C_e}\right)=a\times\ln V-a\times\ln\left(\frac{q_{d-r}\times m}{C_o}\right)$	Constants a and q_o were determined from a plot (plot omitted) of $\ln(C_e/C_o-C_e)$ vs. V. Where $V=Q\times t$, Q is the flow rate
(8)	Weibull distribution	$\ln\left[-\ln\left(1-\frac{C_e}{C_o}\right)\right]=\beta\ln(t)-\beta\ln(\alpha)$	Values of β and α are obtained from the slope and intercept of the linear plots (plot omitted) of $\ln[-\ln(1-C_e/C_o)]$ vs. $\ln(t)$

The Weibull function is similar to the Bohart–Adams model in several respects, both consider sigmoid or *S*-shaped curves. Their simple mathematical shapes can be linearized and then linear regression can be used to estimate the parameters. The Weibull distribution is very effective in analyzing the highly skewed advanced data form of fixed-bed column adsorption [21]. In this work, it has been proposed to link the two empirical parameters in relation to the volumetric flow. Where the constant of the Weibull distribution "β" has the unit min^{-1} and the value of "α" is related to the adsorption capacity as follows: $\alpha = q_W m/C_o Q$. The maximum adsorption capacity (q_W) can be calculated with this relationship from the model.

The results from the Weibull distribution are very similar to the Thomas and Dose–Response models, the constants increase with increasing adsorbent mass. The determination coefficient R^2 shows a good fit of the experimental values to the model.

The four applied models adjusted satisfactorily to the experimental data; all the models have shown values for the determination coefficient (R^2) from 92.68 to 99.24. These values showed that the adsorption process followed Langmuir kinetics of adsorption–desorption [42].

Furthermore, in the case of the Weibull distribution, the adsorption capacity is similar to those values calculated with all other models, around 1.4 ± 0.12 (mg/g). Therefore, it can be assumed that this model can describe the mechanism of the adsorption process in a dynamic system.

The Dose–Response model is the one that best describes the experimental data, with R^2 values of 0.99 and 0.98 for 0.5 and 1.0 g, respectively.

Through a non-linear regression analysis, it was found that the experimental data fit the models, as can be seen in Fig. 6. In general, the breakthrough curves predicted by the models were very similar to each other.

3.3.3. Column operating parameters

Small-scale column tests can be used to simulate the potential performance of the adsorbent and extrapolate the results obtained to a pilot scale or larger. The equations to determine the operational parameters of the column and their results are presented in Tables 4 and 5, respectively.

The operating capacity of the activated biomaterial (*Luffa cylindrica*-HA) can be estimated using the equations shown in Table 4, and the results are shown in Table 5.

The bed volume is the number of liters of feedwater containing F^- (mg/L) that can be adsorbed with one mass of bed. Considering volumes (4.32 and 8.64 cm^3), total weights (0.5 and 1.0 g), and heights (5.5 and 11.0 cm) of the beds, the bed volumes obtained are 71.8 and 69.3, respectively.

The adsorbent exhaustion rate was found by dividing the mass of the adsorbent used by the volume of treated water at the breakthrough point, (90%). Thus, it is defined as the mass of the adsorbent depleted for each volume of liquid treated in the breakthrough curve (30% or 90%).

The residence time in the bed increased and the bio-adsorbent depletion rate was constant for both weights. The results indicate that the longer the residence time and a constant depletion rate, the more efficient the adsorption process.

3.3.4. Adsorption mechanism

Physical adsorption (electrostatic interaction) and chemical adsorption (ion-exchange) are the adsorption mechanisms of fluoride ions on hydroxyapatite particles that are mentioned in different works [10,21,48,49].

The sorption phenomenon is a combination of exchange adsorption, van der Waals force adsorption and chemical adsorption. Exchange adsorption can be assumed because fluoride ions are concentrated on the surface of the adsorbent, which is electrically charged. If the adsorbent is loaded with hydroxyapatite, the hydroxides present may be displaced, and the fluoride ions adsorbed.

In the process of exchange adsorption, fluoride ions with hydroxyapatite release OH^-, changing the pH of the solution after reaction. As shown in Fig. 7, the pH of the solution increased with contact time and reached equilibrium at 390 min.

In the FTIR spectrum of activated *Luffa cylindrica* (Fig. 4a), a new peak appears at 3,652 cm^{-1}, which can be attributed to the OH^- band, specific for hydroxyapatite and possibly, when interacting with fluoride ions, it will form fluorhydroxyapatite.

The ion-exchange reaction between HA and fluoride ions can be observed in the following equation [21]:

$$Ca_{10}(PO_4)_6(OH)_2 + F^- \rightarrow Ca_{10}(PO_4)_6(F,OH) + OH^- \quad (5)$$

On the other hand, the charge distribution of the support material (*Luffa cylindrica*), when activated with HA,

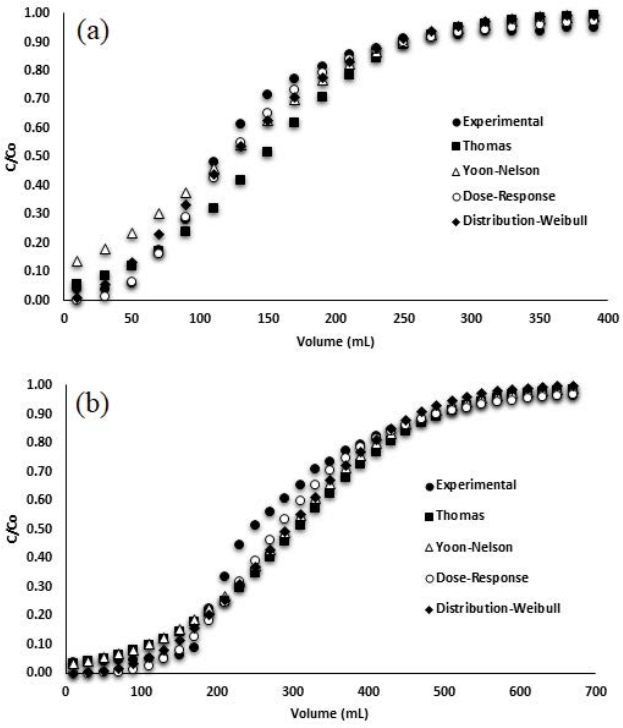

Fig. 6. Models of Thomas, Yoon–Nelson, Dose–Response, and Weibull distribution fits compared to the experimental fluoride breakthrough curve with bed weight of 0.5 and 1.0 g.

Table 4
Summary of the equations used to determine the operational parameters [49]

No.	Equations	Nomenclature
(9)	$\text{BV} = \frac{\text{volume of treated solution}}{\text{volume of the bioadsorbent bed}}$	Numbers for bed volume (BV)
(10)	$\text{BER} = \frac{\text{mass of bioadsorbent}}{\text{treated volume at exhaustion time}}$	Bioadsorbent exhaustion rate (BER)
(11)	$\text{EBRT} = \frac{\text{bed volume}}{\text{volumetric flow rate}}$	Empty bed residence time (EBRT)
(12)	$q_{t_e} = \frac{Q_V t_e C_o}{m}$	(t_e) is the service time in the exhausted column (min); C_o is the inlet ion's initial concentration (mg/L); Q_V is the effluent volumetric flow rate (L/min); m is the amount of bioadsorbent (g)
(13)	$q_e = \frac{M_r}{m}$	m is the mass of bioadsorbent (g); M_r is the influent fluoride load-mass of fluoride, escaping from the column
	$M_r = V_e C_o - \sum \frac{\left(V_{n+1} - V_n\right)\left(C_{n+1} - C_n\right)}{2}$	C_o is the initial fluoride concentration (mg/L); V_e is the volume at the time when the column is exhausted (L); V_n is the throughput volume at the nth reading (L); V_{n+1} is the throughput volume at the (n + 1) nth reading (L); C_n is the fluoride concentration at the nth reading (mg/L); C_{n+1} is the effluent fluoride concentration at the (n + 1) the reading (mg/L)
(14)	$A = \sum \frac{\left(V_{n+1} - V_n\right)\left(C_{n+1} - C_n\right)}{2}$	A is the area under the breakthrough curve, signifies the mass of fluoride ion that was not eliminated, which was estimated as a function of volume and calculated from the breakthrough curves using a Microsoft Excel spreadsheet

Table 5
Parameters for both bed weights

Parameters	Bed weight (g)	
	0.5	1.0
t_p (min)	92.0	202.7
t_e (min)	243.3	490.0
BV processed	71.8	69.3
$\text{BER}_{90\%}$ (g/L)	2.1	2.1
EBRT (min)	4.3	8.6
q_{te} (mg/g)	2.4	2.4
q_e (mg/g)	2.4	2.4

(t_p) Breakthrough time at 30%; (t_e) breakthrough time at 90%

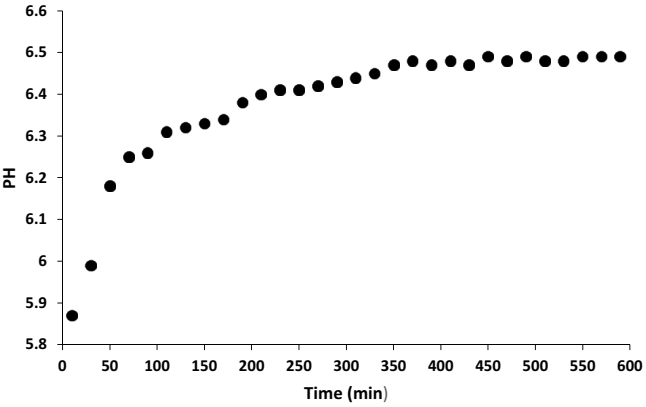

Fig. 7. pH vs. time in the adsorption process of fluoride ions by *Luffa cylindrica*-HA.

increases the active sites, giving place to interaction between the solute and the adsorbent. It can be proposed that both adsorption mechanisms may take place in the system studied in this work.

3.3.5. Desorption of fluoride ions from Luffa cylindrica-HA

Desorption experiments were conducted to examine the reusability of the *Luffa cylindrica*-HA and the reversibility of the adsorption process. A low percentage of desorption (<2.5%) was observed, this behavior suggests that fluoride ions cannot be easily removed from the adsorbent surface by ion-exchange with OH^- ions. The small amount of fluoride ions detected in solution after desorption is possibly due to the formation of chemical bonds between the fluoride and the surface of the *Luffa cylindrica*-HA that prevent the fluoride from being easily desorbed.

4. Conclusions

Biomaterials were synthesized by a simple deposition/reduction technique and used for the removal of fluoride ions from aqueous solution. The bioadsorbent *Luffa cylindrica*-HA presented the highest adsorption capacity (0.49 mg F^-/g biomaterial). Through a linear and non-linear regression analysis, it was found that the experimental data fit well different models from the literature, confirming the

validity of the experimental data. The Weibull distribution gave a good prediction of the fixed-bed column adsorption ($R^2 \geq 0.95$). Therefore, it can be assumed that this model can describe the adsorption process in a dynamic system. The Dose–Response model was the one that best reproduced the experimental breakthrough curves. With the data obtained from the kinetic and scale-up methods, it would be possible to calculate the design parameters for a fixed-bed column on a pilot scale. The *Luffa cylindrica*-HA demonstrated to be effective and a biocompatible adsorbent for fluoride removal from water and scaling up to a pilot level is feasible.

Acknowledgments

The authors thank the Tecnológico Nacional de México for the financial support.

References

[1] S.J. Kashyap, R. Sankannavar, G.M. Madhu, Fluoride sources, toxicity and fluorosis management techniques – a brief review, J. Hazard. Mater. Lett., 2 (2021) 100033, doi: 10.1016/j.hazl.2021.100033.
[2] X. Meng, Y. Yao, Y. Ma, N. Zhong, S. Alphonse, J. Pei, Effect of fluoride in drinking water on the level of 5-methylcytosine in human and rat blood, Environ. Toxicol. Pharmacol., 81 (2021) 103511, doi: 10.1016/j.etap.2020.103511.
[3] S. Budyanto, Y.L. Kuo, J.C. Liu, Adsorption and precipitation of fluoride on calcite nanoparticles: a spectroscopic study, Sep. Purif. Technol., 150 (2015) 325–331.
[4] N.A. Oladoja, S. Chen, J.E. Drewes, B. Helmreich, Characterization of granular matrix supported nano magnesium oxide as an adsorbent for defluoridation of groundwater, Chem. Eng. J., 281 (2015) 632–643.
[5] N. Ben Grich, A. Attour, M. Le Page Mostefa, S. Guesmi, M. Tlili, F. Lapicque, Fluoride removal from water by electrocoagulation: effect of the type of water and the experimental parameters, Electrochim. Acta, 316 (2019) 257–265.
[6] J. Shen, A. Schäfer, Removal of fluoride and uranium by nanofiltration and reverse osmosis: a review, Chemosphere, 117 (2014) 679–691.
[7] P. Pillai, S. Dharaskar, S. Pandian, H. Panchal, Overview of fluoride removal from water using separation techniques, Environ. Technol. Innovation, 21 (2021) 101246, doi: 10.1016/j.eti.2020.101246.
[8] K. Wan, L. Huang, J. Yan, B. Ma, X. Huang, Z. Luo, H. Zhang, T. Xiao, Removal of fluoride from industrial wastewater by using different adsorbents: a review, Sci. Total Environ., 773 (2021) 145535, doi: 10.1016/j.scitotenv.2021.145535.
[9] J. He, Y. Yang, Z. Wu, C. Xie, K. Zhang, L. Kong, J. Liu, Review of fluoride removal from water environment by adsorption, J. Environ. Chem. Eng., 8 (2020) 104516, doi: 10.1016/j.jece.2020.104516.
[10] J. He, K. Zhang, S. Wu, X. Cai, K. Chen, Y. Li, B. Sun, Y. Jia, F. Meng, Z. Jin, L. Kong, J. Liu, Performance of novel hydroxyapatite nanowires in treatment of fluoride contaminated water, J. Hazard. Mater., 303 (2016) 119–130.
[11] A. Jeyaseelan, K.M.M. Katubi, N.S. Alsaiari, M. Naushad, N. Viswanathan, Design and fabrication of sulfonic acid functionalized graphene oxide for enriched fluoride adsorption, Diamond Relat. Mater., 117 (2021) 108446, doi: 10.1016/j.diamond.2021.108446.
[12] S. Raghav, P. Jain, D. Kumar, Assembly of cerium impregnated pectin/silica–gel biopolymeric material for effective utilization for fluoride adsorption studies, Mater. Today Proc., 50 (2022) 273–281.
[13] R. Mudzielwana, M.W. Gitari, Removal of fluoride from groundwater using MnO_2 bentonite-smectite rich clay soils composite, Groundwater Sustainable Dev., 14 (2021) 100623, doi: 10.1016/j.gsd.2021.100623.
[14] N.G. Corral-Capulin, A.R. Vilchis-Nestor, E. Gutiérrez-Segura, M. Solache-Ríos, Comparison of the removal behavior of fluoride by Fe^{3+} modified geomaterials from water, Appl. Clay Sci., 173 (2019) 19–28.
[15] R.W. Premathilaka, N.D. Liyanagedera, Fluoride in drinking water and nanotechnological approaches for eliminating excess fluoride, J. Nanotechnol., 2019 (2019) 2192383, doi: 10.1155/2019/2192383.
[16] C. Sairam Sundaram, N. Viswanathan, S. Meenakshi, Fluoride sorption by nano-hydroxyapatite/chitin composite, J. Hazard. Mater., 172 (2009) 147–151.
[17] G. Patel, U. Pal, S. Menon, Removal of fluoride from aqueous solution by CaO nanoparticles, Sep. Sci. Technol., 44 (2009) 2806–2826.
[18] J. Kang, B. Li, J. Song, D. Li, J. Yang, W. Zhan, D. Liu, Defluoridation of water using calcined magnesia/pullulan composite, Chem. Eng. J., 166 (2011) 765–771.
[19] X. Zhao, J. Wang, F. Wu, T. Wang, Y. Cai, Y. Shi, G. Jiang, Removal of fluoride from aqueous media by Fe_3O_4@$Al(OH)_3$ magnetic nanoparticles, J. Hazard. Mater., 173 (2010) 102–109.
[20] Q. Liu, H. Guo, Y. Shan, Adsorption of fluoride on synthetic siderite from aqueous solution, J. Fluorine Chem., 131 (2010) 635–641.
[21] D. Zhang, H. Luo, L. Zheng, K. Wang, H. Li, Y. Wang, H. Feng, Utilization of waste phosphogypsum to prepare hydroxyapatite nanoparticles and its application towards removal of fluoride from aqueous solution, J. Hazard. Mater., 241–242 (2012) 418–426.
[22] M. Tariq, U. Farooq, M. Athar, M. Salman, M. Tariq, S. Shahida, Z.H. Farooqi, Lab-scale continuous flow studies for comparative biosorption of cadmium(II) on untreated and xanthated *Ficus religiosa* biomass, Water Environ. Res., 93 (2021) 2681–2695.
[23] K.H. Chu, Fixed-bed adsorption of chromium and the Weibull function, J. Hazard. Mater. Lett., 2 (2021) 100022, doi: 10.1016/j.hazl.2021.100022.
[24] G. Yan, T. Viraraghavan, M. Chen, A new model for heavy metal removal in a biosorption column, Adsorpt. Sci. Technol., 19 (2001) 25–43.
[25] I.O. Mazali, O.L. Alves, Morphosynthesis: high fidelity inorganic replica of the fibrous network of loofa sponge (*Luffa cylindrica*), An. Acad. Bras. Cienc., 77 (2005) 25–31.
[26] R. Babou-Kammoe, S. Hamoudi, F. Larachi, K. Belkacemi, Synthesis of $CaCO_3$ nanoparticles by controlled precipitation of saturated carbonate and calcium nitrate aqueous solutions, Can. J. Chem. Eng., 90 (2012) 26–33.
[27] A.S.S. Nila, Synthesis and XRD, FTIR studies of alumina nanoparticle using co-precipitation method, Int. J. Res. Appl. Sci. Eng. Technol., 6 (2018) 2493–2496.
[28] R. Yuvakkumar, V. Elango, V. Rajendran, N. Kannan, Preparation and characterization of zero valente iron nanoparticles, Dig. J. Nanomater. Biostruct., 6 (2011) 1771–1776.
[29] B.W. Lee, Preparation of hydroxyapatite by aqueous precipitation from calcium carbonate and phosphoric acid, IOP Conf. Ser.: Mater. Sci. Eng., 1113 (2021) 012013.
[30] D. Moret-Fernández, M.V. López, Un Método sencillo para la estimacion de la porosidad de un agregado de suelo DE, S. Martínez, A. Sastre, Eds., Estud. En La Zo. No Saturada. XII ZNS'15 (2015) 3–6. Available at: http://hdl.handle.net/10261/136762
[31] J.J. García-Sánchez, V. Martínez-Miranda, M. Solache-Ríos, Aluminum and calcium effects on the adsorption of fluoride ions by corrosion products, J. Fluorine Chem., 145 (2013) 136–140.
[32] H. Gheisari, E. Karamian, M. Abdellahi, A novel hydroxyapatite–hardystonite nanocomposite ceramic, Ceram. Int., 41 (2015) 5967–5975.
[33] A. Chandrasekar, S. Sagadevan, A. Dakshnamoorthy, Synthesis and characterization of nano-hydroxyapatite (n-HAP) using the wet chemical technique, Int. J. Phys. Sci., 8 (2013) 1639–1645.

[34] M. Yu, C. He, H. Zhang, R. Hou, J. Xue, Effect of different pretreatments on tribological properties of wheat straw/polypropylene composites, Nongye Jixie Xuebao = Trans. Chinese Soc. Agric. Mach., 44 (2013) 138–143.
[35] S. Mishra, G. Sen, Microwave initiated synthesis of polymethylmethacrylate grafted guar (GG-g-PMMA), characterizations and applications, Int. J. Biol. Macromol., 48 (2011) 688–694.
[36] S. Kalia, A. Kumar, B.S. Kaith, Sunn hemp cellulose graft copolymers polyhydroxybutyrate composites: morphological and mechanical studies, Adv. Mater. Lett., 2 (2011) 17–25.
[37] S.S. Saravanakumar, A. Kumaravel, T. Nagarajan, P. Sudhakar, R. Baskaran, Characterization of a novel natural cellulosic fiber from *Prosopis juliflora* bark, Carbohydr. Polym., 92 (2013) 1928–1933.
[38] V.O.A. Tanobe, T.H.D. Sydenstricker, M. Munaro, S.C. Amico, A comprehensive characterization of chemically treated Brazilian sponge-gourds (*Luffa cylindrica*), Polym. Test., 24 (2005) 474–482.
[39] Y. Wang, X.-Y. Shen, Optimum plasma surface treatment of luffa fibers, J. Macromol. Sci. Part B Phys., 51 (2012) 662–670.
[40] WHO, Guidelines for Drinking-Water Quality: Fourth Edition Incorporating the First Addendum, 2017, pp. 370–373. Available at: https://www.ncbi.nlm.nih.gov/books/NBK442376/ (Accessed October 9, 2021).
[41] H.C. Thomas, Heterogeneous ion-exchange in a flowing system, J. Am. Chem. Soc., 66 (2002) 1664–1666.
[42] J.J. García-Sánchez, M. Solache-Ríos, V. Martínez-Miranda, R. Enciso-Perez, N.V. Arteaga-Larios, M.C. Ojeda-Escamilla, I. Rodríguez-Torres, Experimental study of the adsorption of fluoride by modified magnetite using a continuous flow system and numerical simulation, Process Saf. Environ. Prot., 109 (2017) 130–139.
[43] Z. Aksu, F. Gönen, Biosorption of phenol by immobilized activated sludge in a continuous packed bed: prediction of breakthrough curves, Process Biochem., 39 (2004) 599–613.
[44] X. Zhang, Y. Li, M. Wu, Y. Pang, Z. Hao, M. Hu, R. Qiu, Z. Chen, Enhanced adsorption of tetracycline by an iron and manganese oxides loaded biochar: kinetics, mechanism and column adsorption, Bioresour. Technol., 320 (2021) 124264, doi: 10.1016/j.biortech.2020.124264.
[45] D. Politi, D. Sidiras, Modified spruce sawdust for sorption of hexavalent chromium in batch systems and fixed-bed columns, Molecules, 25 (2020) 5156, doi: 10.3390/molecules25215156.
[46] L.M. Vera-Cabezas, D. Bermejo-Campos, M.F. Uguña-Rosas, N. García-Alvear, M. Flores-Zamora, D. Brazales, L.M. Vera-Cabezas, D. Bermejo-Campos, M.F. Uguña-Rosas, N. García-Alvear, M. Flores-Zamora, D. Brazales, Modelado en columna de lecho fijo para la bioadsorción de Cd^{2+} Y Pb^{2+} con cáscara de cacao, Rev. Int. Contam. Ambient., 34 (2018) 611–620.
[47] J.J. García-Sánchez, M. Solache-Ríos, M.T. Alarcón-Herrera, V. Martínez-Miranda, Removal of fluoride from well water by modified iron oxides in a column system, Desal. Water Treat., 57 (2016) 2125–2133.
[48] C.S. Sundaram, N. Viswanathan, S. Meenakshi, Defluoridation chemistry of synthetic hydroxyapatite at nano scale: equilibrium and kinetic studies, J. Hazard. Mater., 155 (2008) 206–215.
[49] Y. Wang, N. Chen, W. Wei, J. Cui, Z. Wei, Enhanced adsorption of fluoride from aqueous solution onto nanosized hydroxyapatite by low-molecular-weight organic acids, Desalination, 276 (2011) 161–168.